Application of polarized neutron reflectometry to studies of artificially structured magnetic materials

M. R. Fitzsimmons
Los Alamos National Laboratory
Los Alamos, NM 87545 USA

and

C.F. Majkrzak
National Institute of Standards and Technology
Gaithersburg, MD 20899 USA

Introduction

Reflectometry involves measurement of the intensity of a beam of electromagnetic radiation or particle waves reflected by a planar surface and/or interfaces. The technique is intrinsically sensitive to the difference of the refractive index (or contrast) across surfaces and interfaces. For the case of specular reflection, i.e., the case when the angle of reflection, α_r, equals the angle of incidence, α_i, [see Figure 1(a)], the intensity of the reflected radiation is related to the depth dependence of the index of refraction averaged over the lateral dimensions of the surface or interface. In this simplest example of reflectometry, the sharpness of an interface can be quantitatively measured, the distance between two or more planar interfaces can be obtained, and the strength of the scattering potential, i.e., the index of refraction, between the interfaces can be measured relative to that of the medium through which the radiation travels to reach the sample surface (in many cases the surrounding medium is air or vacuum—for neutron scattering there is little distinction). In more complex situations, variations of the refractive index within the plane of the interface may give rise to diffuse scattering or off-specular reflectivity, i.e., radiation reflected away from the specular condition [see Figure 1(b and c)]. From measurements of off-specular reflectivity, correlations between lateral variations of the scattering potential along an interface can be deduced. Off-specular scattering introduces a component of wavevector transfer in the plane of the sample mostly parallel to the incident neutron beam [Figure 1(b)] [1] or perpendicular to it [Figure 1(c)] [23].

Figure 1 Scattering geometry for (a) specular reflectometry, where $\alpha_r = \alpha_i$, (b) off-specular reflectometry where $\alpha_r \neq \alpha_i$, and (c) glancing incidence diffraction where $2\theta \neq 0$. The components of wavevector transfer, $Q = k_f - k_i$ are shown for each scattering geometry.

So far, the capabilities of reflectometry have been described without regard to the

kind of radiation used. Many detailed discussions of X-ray [4, 5, 6, 7, 8, 9, 10] and

unpolarized neutron reflectometry [10, 11] from non-magnetic materials can be found in

the literature. Treatments of X-ray reflectometry invariably use concepts of optics and Maxwell's equations. Treatments of neutron reflectometry can be optical in nature, but often treat the neutron beam as a particle wave and use quantum mechanics to calculate reflection and transmission probabilities across interfaces bounding potential wells. In the present chapter, we focus on reflectometry of magnetic thin films and artificially structured magnetic materials using polarized neutron beams.

Polarized neutron reflectometry is a tool to investigate the magnetization profile near the surfaces of crystals, thin films and multilayers. Surface (or interface) sensitivity derives from working in glancing incidence geometry near the angle for total external reflection. Polarized neutron reflectometry is highly sensitive, having measured the absolute magnetization of a monolayer of iron ($\sim 10^{-4}$ emu) with 10% precision [12], and magnetization density as small as 30 emu/cm^3 (e.g., as found in $Ga_{0.97}Mn_{0.3}As$) with comparable precision. Detection of small moments (from samples with surfaces measuring a ~ 4 cm^2 in area) is combined with excellent depth resolution—a fraction of a nanometer even for films as thick as several hundred nanometers. Reflectometry has enjoyed dramatic growth during the last decade and has been applied to important problems such as, the influence of frozen or pinned magnetization on the origin of exchange bias [13], the influence of exchange coupling on magnetic domain structures [14, 15], and the identification of spatially inhomogeneous magnetism in nanostructured systems [16, 17, 18].

Several descriptions of polarized neutron reflectometry are available in the literature [19, 20, 21, 22, 23, 24, 25]. Recently reviews of polarized neutron reflectometry, one that includes illustrative examples [26], and a second very detailed

account of the scattering of polarized neutron beams, with copious mathematical derivations of formulae, have been published [27,28]. In this chapter, we present a tutorial on polarized neutron reflectometry, a description of a polarized neutron reflectometer at a pulsed neutron source, and examples of applications of the technique.

Neutron scattering in reflection (Bragg) geometry

Reflectometry with unpolarized neutron beams

In Figure 2, we show the general situation for a neutron beam with wavelength λ represented by a plane wave in air (Medium 0) with incident wavevector $\mathbf{k_i}$ ($|\mathbf{k_i}| = k_0 = 2\pi/\lambda$) and reflected wavevector $\mathbf{k_f}$ (reflected by the sample, Medium 1). A portion of the plane wave is transmitted across the reflecting interface with wavevector $\mathbf{k_t}$. Depending upon the distribution of chemical or magnetic inhomogenities in the plane of the sample, neutron radiation can be scattered in directions such that $2\theta \neq 0$ and/or $\alpha_r \neq \alpha_i$ [see Figure 1]. The case of elastic and specular ($2\theta = 0$ and $\alpha_r = \alpha_i$) reflection is the simplest to treat. Neutron scattering is called elastic when the energy $E = \dfrac{\hbar^2 k_0^2}{2m_n}$ of the neutron is conserved. Thus, the magnitudes of $\mathbf{k_i}$ and $\mathbf{k_f}$ are equal, i.e., $|\mathbf{k_i}| = |\mathbf{k_f}|$. The magnitude of $\mathbf{k_t}$ in Medium 1, $|\mathbf{k_t}| = k_1$, may be (and usually is) different than that of Medium 0.
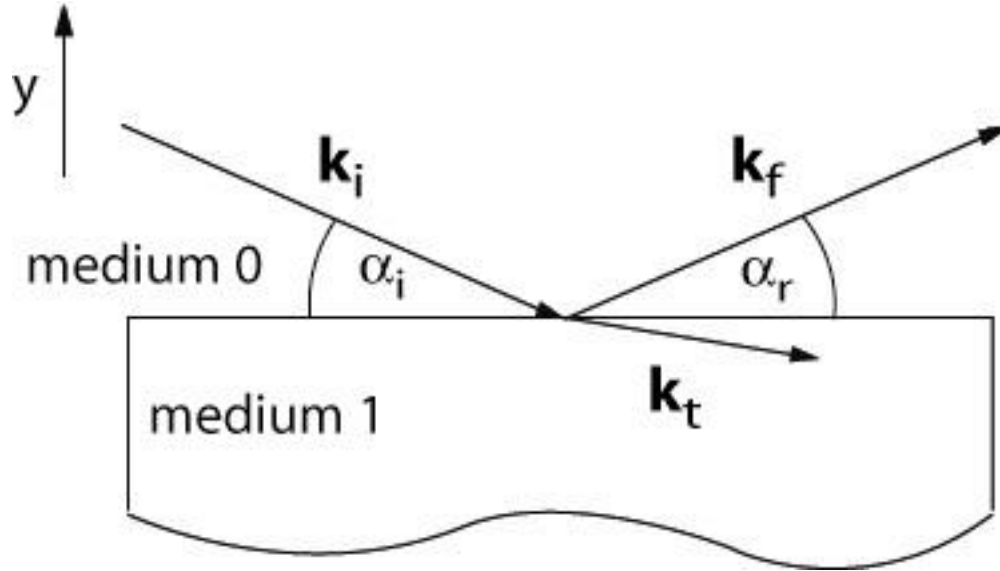
Figure 2 Schematic diagram showing the incident, reflected and transmitted wavevectors. The sample in this case is Medium 1.

The quantity measured in a neutron reflectometry experiment is the intensity of the neutron beam reflected from the surface. The probability of reflection or the reflectivity is given by the reflected intensity divided by the incident intensity. To calculate the reflectivity of an interface, we apply the time-independent Schrödinger equation [29] to obtain a solution for the wave function, Ψ, representing the neutron wave inside and outside of the reflecting sample. Dropping the parts of the wave function with wavevector components parallel to the interface (we consider a potential that varies in only one dimension which cannot change the neturon's wavevector parallel to the interface), the wave functions in mediums 0 and 1 are given by:

$$\Psi_0(y) = e^{+ik_0 y} + re^{-ik_0 y}$$
$$\Psi_1(y) = te^{+ik_1 y}$$

Equation 1

Unless otherwise noted, k_i is the $\perp$–component of the wavevector $\boldsymbol{k}_i$.

The neutron reflectivity, R, of the interface is related to the reflection amplitude, r, by $R = rr^*$. Ψ is obtained by solving Schrödinger's equation:

$$\left[\frac{\hbar^2}{2m_n} \frac{\partial^2}{\partial y^2} + V(y) \right] \Psi(y) = E\Psi(y)$$

Equation 2

where V(y) is the depth dependent scattering potential. For a planar sample, the neutron (nuclear) scattering potential is represented by the expression:

$$V_n = \frac{2\pi\hbar^2}{m_n} \rho(y)$$

Equation 3

where ρ(y) is the neutron scattering length density in units of $Å^{-2}$. Owing to the decay in the strength of the reflected neutron beam with wavevector transfer (discussed later), neutron reflectometry usually involves measurements that are restricted to fairly small wavevector transfer, $Q_\perp < 0.3$ Å. Over this range of $Q_\perp$, the scattering medium can be considered to consist of a continuous scattering length density of N (scattering centers or formula units per unit volume) each with coherent neutron scattering length b. For systems composed of a mixture of elements or formula units,

$$\rho = \sum_i^J N_i b_i$$

Equation 4

where J is the number of distinct isotopes, and N_i and b_i are the number density and scattering length for the i-th species. Values of N, b and ρ are given for a number of common materials in Table 1 30.

Invoking the condition of elastic scattering, Equation 2 can be rewritten as:

$$\left[\frac{\partial^2}{\partial y^2} + k_0^2 - 4\pi\rho(y) \right]\Psi(y) = 0$$

<div align="right">**Equation 5**</div>

In the language of ordinary light optics, the $\perp$-component of the wavevector in Medium 1, k_1, is related to the $\perp$-component of the wavevector in Medium 0, k_0, through the index of refraction, n, by

$$k_1 = nk_0 = \sqrt{1 - \frac{4\pi\rho}{k_0^2}}k_0$$

<div align="right">**Equation 6**</div>

During an experiment, the intensity of the reflected radiation is measured for selected values of k_0, which are chosen either by changing the angle of incidence of the beam to the sample surface, α_i, and/or by changing the wavelength, λ, of the neutron beam. For sufficiently small values of k_0, the index of refraction will be imaginary, so the neutron wave in Medium 1 is evanescent (the wave does not loose energy to Medium 1 [31]). Therefore, the wave is reflected by the sample with unit probability. The wavevector transfer $Q_\perp$ at which n obtains a real component is the called the critical edge, Q_c. For $Q_\perp < Q_c$, the reflected intensity is unity, and provides a means to normalize the reflectivity to an absolute scale (in contrast to small angle neutron scattering). Since the reflectivity of the sample is unity below Q_c, the scattering in this region is strong, so a dynamical treatment of the scattering is required. By dynamical, we mean the wave function inside Medium 1 is not the same as that illuminating the sample. Because the Born approximation [29] is a perturbation theory, it is valid for weak scattering, e.g., small-angle neutron scattering in transmission geometry, so this approximation is not

adequate for calculating reflection of neutrons or X-rays at glancing angles from planar or nearly planar interfaces.

Table 1 Listing of common elements and their neutron nuclear and magnetic scattering length densities.

Material	Number density, N [Å^{-3}]	Nuclear scattering length, b [Å]	Magnetic moment, μ [μ_B]	Nuclear scattering length density, ρ_n [Å^{-2}]	Magnetic scattering length density, ρ_m [Å^{-2}]
Ag	5.86×10^{-2}	5.92×10^{-5}		3.47×10^{-6}	
Al	6.02	3.45		2.08	
Al_2O_3	2.13	24.4		5.21	
Au	5.90	7.90		4.66	
Co	9.09	2.49	1.715	2.26	4.12×10^{-6}
Fe	8.47	9.45	2.219	8.00	4.97×10^{-6}
FeF_2	2.75	20.76		5.71	
Fe_2O_3 (hematite)	2.00	36.32		7.26	
Fe_3O_4	1.35	51.57	4.1	6.97	1.46×10^{-6}

(magnetite)					
GaAs	2.21	13.87		3.07	
LaAlO$_3$	1.84	29.11		5.34	
LaFeO$_3$	1.65	35.11		5.78	
LaMnO$_3$	1.71	21.93		3.75	
MgF$_2$	3.07	16.68		5.12	
MgO	5.35	11.18		5.98	
MnF$_2$	2.58	7.58		1.96	
Nb	5.44	7.05		3.84	
Ni	9.13	10.3	0.604	9.40	1.46×10^{-6}
^{58}Ni	9.13	14.4	0.604	13.14	1.46×10^{-6}
^{62}Ni	9.13	-8.7	0.604	-7.94	1.46×10^{-6}
Ni$_{81}$Fe$_{19}$	8.93	10.14	1.04	9.06	2.46×10^{-6}
NiO	5.49	16.11		8.84	
Pd	6.79	5.91		4.01	

Pt	6.60	9.60		6.34	
Pu	4.88	5.8±2.3		2.8±1.1	
Si	4.99	4.15		2.07	
SiO$_2$	2.66	15.76		4.19	
SrTiO$_3$	1.68	21.00		3.54	
U	4.82	8.417		4.06	
V	6.18	-0.38		-0.23	

Theoretical Example 1: Reflection from a perfect interface surrounded by two media of infinite extent

The goal of a reflection experiment is to determine the distribution of material within the sample from measurements of the sample reflectivity as a function of $Q_\perp$. To accomplish this goal, we need to determine the probabilities that the wave function is reflected and transmitted by the sample. Conservation of neutron intensity, i.e., $|\Psi|^2 = 1$, and conservation of momentum require that $\Psi(y)$ and its derivative, $\dfrac{\partial \psi}{\partial y}$, be continuous across the interface. Thus,

$$\begin{pmatrix} \Psi_0(0) \\ \left. \dfrac{\partial \Psi_0}{\partial y} \right|_{y=0} \end{pmatrix} = \begin{pmatrix} \Psi_1(0) \\ \left. \dfrac{\partial \Psi_1}{\partial y} \right|_{y=0} \end{pmatrix} \Rightarrow \begin{pmatrix} 1+r \\ ik_0(1-r) \end{pmatrix} = \begin{pmatrix} t \\ ik_1 t \end{pmatrix}$$

Equation 7

Solving Equation 7 for r, the reflection amplitude of a single interface between two media of infinite extent, gives:

$$r = \left(\frac{k_0 - k_1}{k_0 + k_1} \right)$$

Equation 8

from which the reflectivity of a single interface is obtained:

$$R = rr^* = \left(\frac{k_0 - k_1}{k_0 + k_1} \right)\left(\frac{k_0 - k_1}{k_0 + k_1} \right)^* = \left(\frac{1-n}{1+n} \right)\left(\frac{1-n}{1+n} \right)^*$$

Equation 9

As an example to illustrate application of Equation 9, we consider the case of an unpolarized neutron beam reflecting from a perfectly smooth silicon substrate (surrounded by air). The neutron scattering length density for Si is $\rho_{Si} = 2.07 \ \text{x} 10^{-6} \ \text{Å}^{-2}$

(obtained from the entries listed in Table 1), and the depth dependence of the scattering

length density profile for the sample is shown in Figure 3(a). The reflectivity versus $Q_\perp$

[Figure 3(b)] is calculated using Equation 9. The position of the critical edge, Q_c, is

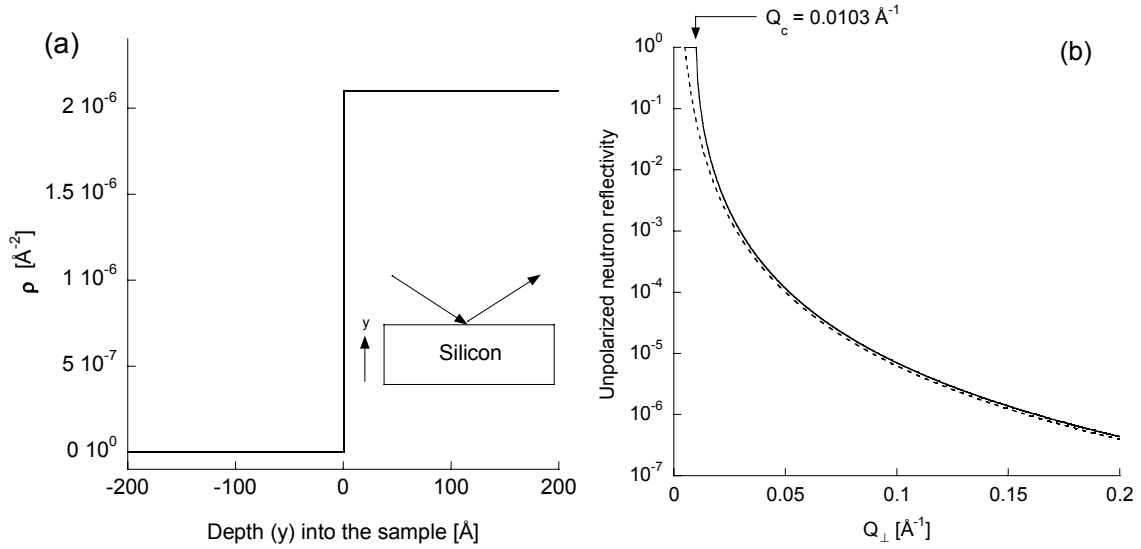determined by the condition $n = 0$, i.e., $Q_c = 4\sqrt{\pi \rho_{Si}}$.

Figure 3 (a) Unpolarized neutron scattering length density profile of a perfect interface between air and a silicon substrate (inset). (b) The calculated reflectivity for the interface (a) is shown by the solid curve. The dashed curve represents a reflectivity curve calculated using the Born approximation (see text) and varies as $Q_\perp^{-4}$ normalized to 0.9 times the solid curve at $Q_\perp = 0.2 \text{Å}^{-1}$ (see text).

The dynamical calculation of the silicon substrate reflectivity [solid curve, Figure

3(b)] in the region of $Q_\perp \sim 0.1 \text{ Å}^{-1}$ is similar to that obtained the Born approximation

(i.e., the kinematical case, dashed curve) from which the reflectivity is equated to the

Fourier transform of the scattering length density profile:

$$R_{BA} \propto \frac{1}{Q_\perp^2} \left| \int_{-\infty}^{\infty} e^{iQ_\perp y} \rho(y) dy \right|^2$$

Equation 10

However, for smaller values of $Q_\perp$ the two reflectivity curves diverge.

15

In the large $Q_\perp$ regime, the decay of the curve scales as $Q_\perp^{-4}$. This decay, called the Fresnel decay [6], is a property of reflection from a planar surface, and thus contains little information leading to a better understanding of the spatial representation of matter beneath the surface. However, the Fresnel decay rapidly diminishes the reflected neutron beam intensity until it can become swamped by external sources of background, including incoherent scattering from the substrate.

Theoretical Example 2: Reflection from perfectly flat stratified media

For the case of reflection from a single perfect interface, there is little additional information that can be obtained beyond that provided by the position of the critical edge (surface roughness can also be measured—a topic discussed later). More interesting and realistic cases involve reflection from stratified media. In these cases, the scattering length density is not constant with depth, and indeed abrupt changes of the scattering length density, such as those produced by buried interfaces, modulate the reflectivity.

Now consider the representation of a stratified sample in Figure 4— one depicting reflection of a neutron beam from a perfect interface formed by the boundary between air and the surface of a thin film with thickness Δ that is in contact with a smooth Si substrate of infinite thickness.
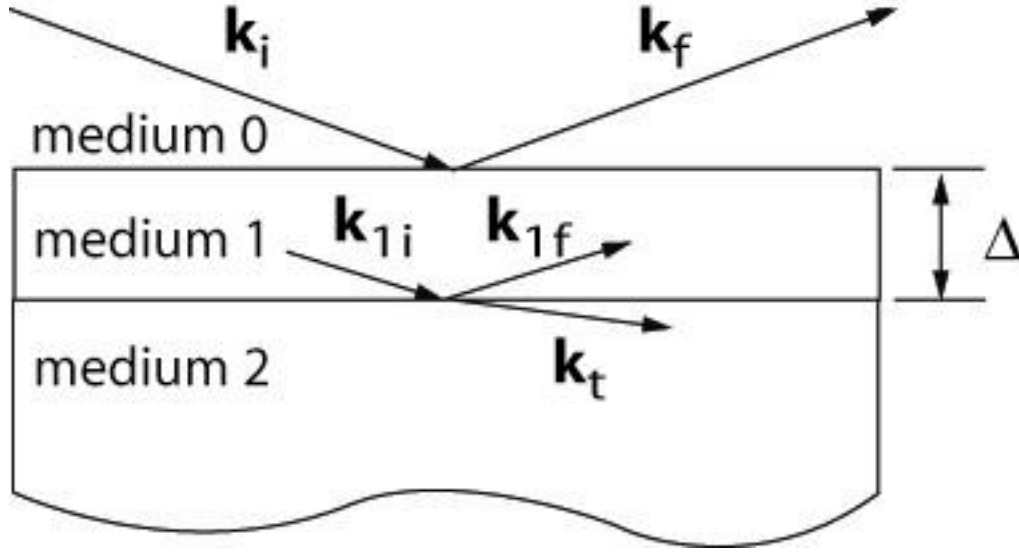
Figure 4 Schematic diagram showing the wavevectors in a stratified medium. The thickness of the thin film is Δ.

The wave functions in the different media are:

$$\Psi_0(y) = e^{+ik_0 y} + re^{-ik_0 y}$$
$$\Psi_1(y) = Ge^{+ik_1 y} + He^{-ik_1 y}$$
$$\Psi_2(y) = te^{+ik_{21} y}$$

<div align="right">**Equation 11**</div>

Again Schrödinger's equation is solved yielding a matrix equation from which the reflection and transmission amplitudes, r and t, can be obtained:

$$\overline{\overline{M_1(\Delta)}} \begin{pmatrix} 1+r \\ ik_0(1-r) \end{pmatrix} = \begin{pmatrix} t \\ ik_2 t \end{pmatrix} e^{ik_2 \Delta}$$

<div align="right">**Equation 12**</div>

and

$$\overline{\overline{M_1(\Delta)}} = \begin{pmatrix} \cos(k_1\Delta) & \dfrac{1}{k_1}\sin(k_1\Delta) \\ -k_1\sin(k_1\Delta) & \cos(k_1\Delta) \end{pmatrix}.$$

<div align="right">**Equation 13**</div>

Equation 12 represents two simultaneous equations that can be solved to obtain r. (Note,

Equation 7 is recovered for the case of a single (air/substrate) interface for the case of $\Delta =$

0.)

$$r = \frac{r_{01} + r_{12}e^{ik_1 2\Delta}}{1 + r_{01}r_{12}e^{ik_1 2\Delta}}$$

$$r_{mn} = \frac{k_m - k_n}{k_m + k_n}$$

$$k_j = n_j k_0 = \sqrt{1 - \frac{4\pi\rho_j}{k_0}} k_0$$

Equation 14

To calculate a reflectivity curve, a value of $Q_\perp$ is chosen from which k_0 (= $Q_\perp/2$, a

real quantity) is obtained. Next, the $\perp$-components of the wavevector in Medium 1 and

Medium 2 are calculated (using Equation 14) from which the reflection amplitudes for a

pair of interfaces are obtained. The reflection amplitudes for an ensemble of interfaces

(in this case two, see Equation 14), r, is related to the reflection amplitudes of each

interface, r_{01} and r_{12} (here, the amplitude of the wave reflected by the interface between

Medium m and Medium n is called r_{mn}), in the ensemble after combination with a phase

factor, $e^{ik_1 2\Delta}$, as appropriate (the wave reflected by the interface between Medium 1 and

Medium 2 is out of phase by the path length 2Δ with respect to the wave reflected by the

interface between Medium 0 and Medium 1). This procedure was performed to obtain

the reflectivity curve (Figure 5) for a sample consisting of a 20 nm thick perfectly flat

layer of material with the nuclear scattering length density of Fe on a perfect Si substrate.
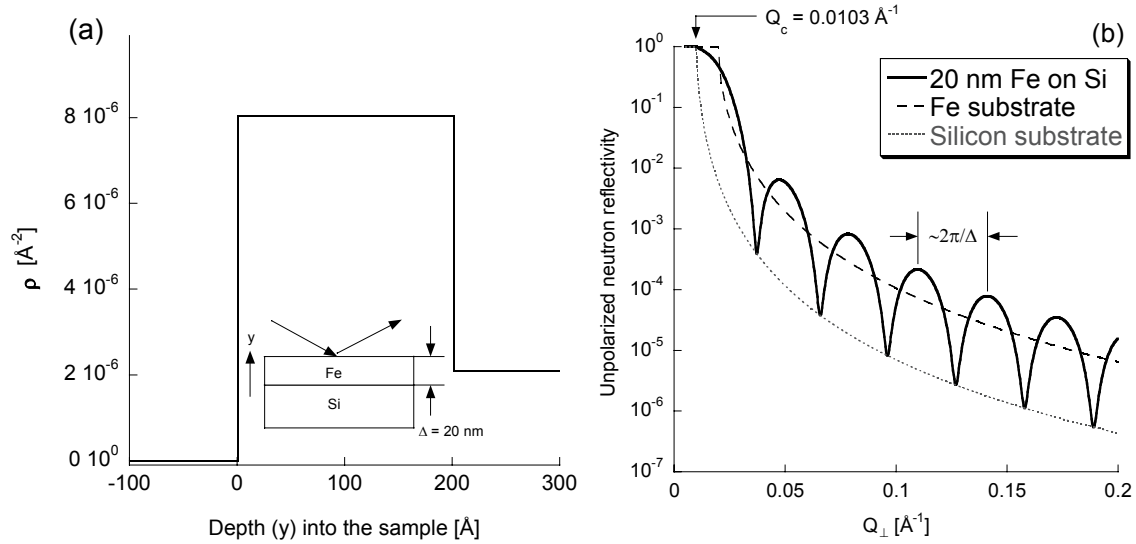
Figure 5 (a) The nuclear scattering length density profile of a perfect thin iron film on silicon (inset). (b)The reflectivity of the sample is shown as the solid curve. The reflectivities of a silicon substrate (dotted curve) and a substrate with the nuclear scattering length density of iron (dashed curve) are shown for comparison.

The most notable feature of the solid curve [Figure 5(b)] is the oscillation of the reflectivity. The period of the oscillation in the kinematical limit (far from the critical edge where dynamic effects are most pronounced) is approximately equal to $2\pi/\Delta$. The amplitude of the oscillation is related to the contrast or difference between the scattering length densities of the iron film and silicon substrate. A second notable feature is the position of the critical edge, which for the 20 nm Fe/Si sample still occurs at a position coinciding with that of the silicon substrate and not at the position for an iron substrate [compare the dotted and dashed curves in Figure 5(b)]. Unlike the case for X-ray reflectometry, in which only a couple of nanometers of material is sufficient to be opaque, and thus create a well-defined critical edge, the critical edge for neutron reflectivity is often determined by the sample substrate, and not the thin film owing to the fact that a neutron beam is a highly penetrating probe.
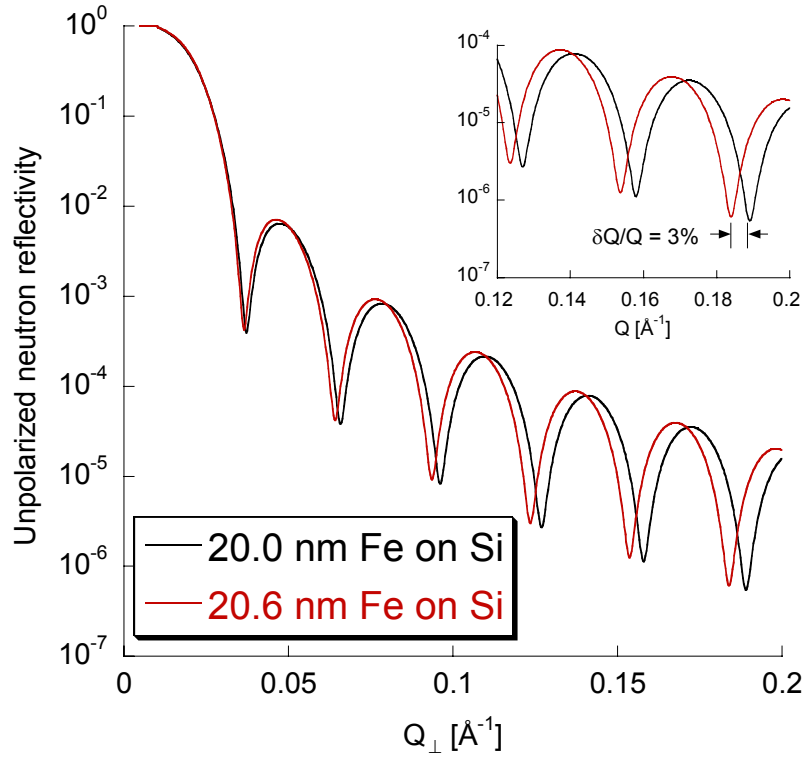
Figure 6 Comparison of reflectivity curves from Fe films with different thicknesses. The difference of 3% in thickness would be easily resolved.

One strength of reflectometry is its ability to measure layer thickness with very high precision and accuracy (for a discussion of the distinction see Ref. [32]). An illustrative example is to compare the calculated reflectivity curves for iron films of 20.0 nm and 20.6 nm thickness— corresponding to a 3% change in film thickness (Figure 6). The shift between the reflectivity curves at large wavevector transfer is easily distinguished, because the resolvable wavevector transfer is smaller than the shift. For small scattering angles, the resolution of a reflectometer, $\delta Q/Q$ is approximately given by:

$$\left(\frac{\delta Q}{Q}\right)^2 = \left(\frac{\delta\theta}{\theta}\right)^2 + \left(\frac{\delta\lambda}{\lambda}\right)^2$$

Equation 15

The first term is determined by a combination of factors including sample size and the dimensions of slits that collimate the incoming neutron beam. For glancing angles of incidence (typically less than 5°), $\delta\theta/\theta$ is of order 2% (root-mean-square). The second term is determined by how well the wavelength of the incident neutron beam is measured. For situations in which a graphite monochromator selects the wavelength (as used for example at a nuclear reactor), $\delta\lambda/\lambda$ is typically 1 to 2% (rms). For situations in which the time-of-flight technique measures neutron wavelength (as used for example at a short pulsed neutron source) $\delta\lambda/\lambda$ is typically 0.2% (rms). So, with little effort, the resolution of a reflectometer in $\delta Q/Q$ can be made less than 3% (rms). Consequently, the change of fringe phase, which is about 3% for the case illustrated in Figure 6, can be readily measured.

In contrast to measuring sub-nanometer changes in film thickness, detection of a single sub-nanometer thick film is considerably more challenging. The Fresnel decay of the reflectivity restricts the degree to which perturbations in the scattering length density profile over thin layers can be measured. Let Q_{max} is the maximum value of $Q_\perp$ that can be measured before the reflectivity, R_{min}, is approximately equal to the instrumental background. Thin films having thickness $\Delta > 2\pi/Q_{max}$ can perturb the reflectivity by superimposing oscillations on the Fresnel decay. In principle, by measuring the period and amplitude of the oscillations, information about the thickness of the thin film and its composition can be inferred. On the other hand, for films with thickness $\Delta < 2\pi/Q_{max}$ the perturbation to the reflectivity might well be missed on account that the first pair of fringe maximum and minimum occur at wavevector transfer so large that the intensity of

the reflected beam is below R_{min} (in other words, the oscillations of the reflectivity curve might be swamped by instrumental background).

Neutron reflectivity has been measured to values of $R_{min} = 10^{-8}$ under ideal conditions. In these conditions, Q_{max} might be on order of 0.3 Å^{-1}, so detection of films as thin as 2 nm might be possible. However, most experiments are not conducted under ideal circumstances. For example, experiments usually involve sample environment equipment, e.g., cryostats etc., or samples that are either not perfectly smooth or are themselves sources of incoherent scattering. In these situations neutron reflectivity measurements to less than 10^{-7} are often not achievable.

Theoretical Example 3: Reflection from "real-world" stratified media

The first two examples of perfect interfaces illustrate the importance of the critical edge (providing a means to place the reflectivity curve on an absolute scale), fringe period (related to layer thickness) and fringe amplitude (related to change of, or contrast between, scattering length density across an interface). Since real systems can be less than perfect, we consider the case of rough or diffused interfaces. This case serves to show how reflectometry can be a useful tool to study systems that are imperfect (indeed reflectometry provides a useful measure of imperfection).

Consider the case where the diffusion of Fe and Si across the Fe/Si interface in the previous example obeys Fick's second law [33]. We further assume the characteristic diffusion length, σ, of Fe into the Si matrix is the same as Si into the Fe matrix (though this assumption is unlikely to be correct). In this case, the concentrations of Fe and Si with depth (in units of atoms/Å^3) are given by:

$$N_{Fe}(y) = N_{Fe}\left[1 - erf\left(\frac{y-\Delta}{\sqrt{2}\sigma}\right)\right]$$

$$N_{Si}(y) = N_{Si}\left[1 + erf\left(\frac{y-\Delta}{\sqrt{2}\sigma}\right)\right]$$

<div align="right">**Equation 16**</div>

After substitution of Equation 16 into Equation 9, and using the appropriate values of the neutron scattering lengths and densities for Fe and Si (see Table 1), the neutron scattering length density profile is obtained:

$$\rho(y) = b_{Fe}N_{Fe} + \frac{b_{Si}N_{Si} - b_{Fe}N_{Fe}}{2}\left[1 + erf\left(\frac{y-\Delta}{\sqrt{2}\sigma}\right)\right]$$

<div align="right">**Equation 17**</div>

The variation of the neutron scattering length density across the interface is represented by an error function connecting the scattering length densities of pure Fe and pure Si. We note the derivative of the error function with argument $\frac{y-\Delta}{\sqrt{2}\sigma}$ is proportional to a Gaussian function with root-mean-square width of σ [34]. The scattering length density profile for a 20 nm thick Fe layer bounded by a diffuse air/Fe surface (i.e., a rough surface) and diffuse Fe/Si interface with characteristic widths of $\sigma =$ 5 Å is shown in Figure 7(a).
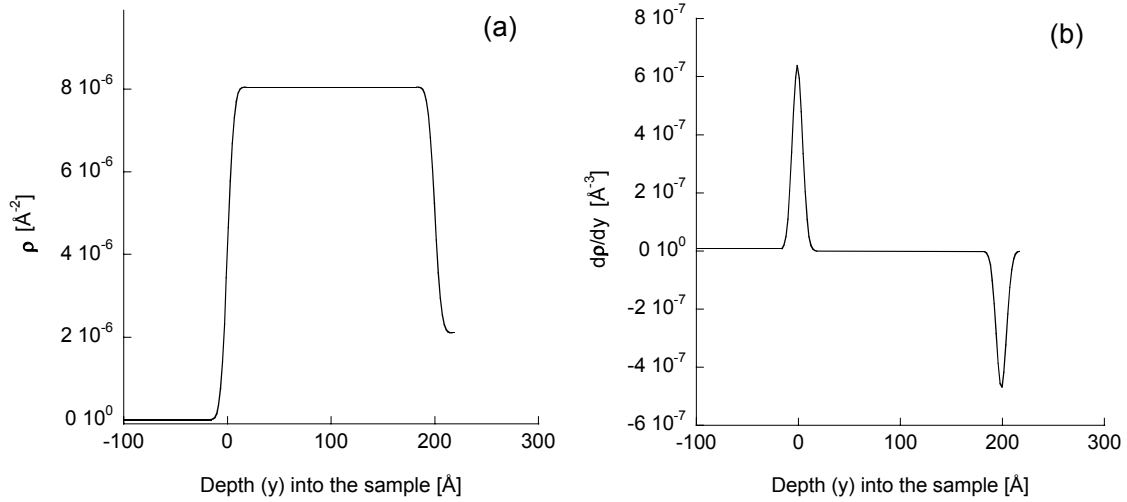
Figure 7 (a) Representation of the Fe/Si sample with rough and/or diffuse interfaces. (b) The derivative of the scattering length density profiles consisting of a pair of Gaussian profiles from which (a) is obtained upon integration.

While the scattering length density profile in Figure 7(a) can be obtained using Equation 17, in fact the profile shown in the figure was obtained by integrating the derivative of the scattering length density profile with respect to depth (y-coordinate) [Figure 7(b)]. The peaks in Figure 7(b) are Gaussian peaks whose positions, widths and integrals correspond to the positions, diffusion or roughness widths, and contrast across the interfaces, respectively. For example, the integral of the peak at y = 0 Å in Figure 7(b) is $\rho_{Fe} - \rho_{air} = 8 \times 10^{-6}$ Å^{-2}. One motivation for constructing the derivative of the scattering length density profile (and then integrating it) is to allow the possibility for interfaces to be positioned close together. By close together we mean the thickness of one or both layers on either side of an interface is thinner than the rms width attributed to the interface. While arguments can be made whether such a situation is physically meaningful, mathematically the situation corresponds to one where tails of adjacent Gaussian peaks overlap, and certainly such a profile can be integrated. When the tails of two Gaussian peaks overlap (significantly), the profile obtained from integrating the

derivative profile will not yield an error function variation between the two interfaces, but may nevertheless produce a calculated reflectivity curve that closely resembles a measured reflectivity. It should be emphasized that only in situations where $\sigma_{mn} << \Delta_m$ and $\sigma_{mn} << \Delta_n$, should the value of σ_{mn} be interpreted as an interface width and Δ as a layer thickness. Otherwise, the parameters of a density profile— ones that yield a well-fitting reflectivity curve, have little meaning, though the density profile might accurately represent the scattering potential of the system.

The process for calculating the reflectivity of the "roughened" sample first involves approximating the continuous profile in Figure 7 by a discrete sequence of thin slabs of width δ with step-like changes in scattering length density. The choice of δ, i.e., the thickness over which ρ is constant, is made such that $\delta << 2\pi/Q_{max}$ —a relation assuring the Sampling Theorem of Fourier analysis [35] is satisfied. An example of such an approximation for $\delta = 2$ Å is shown in Figure 8.

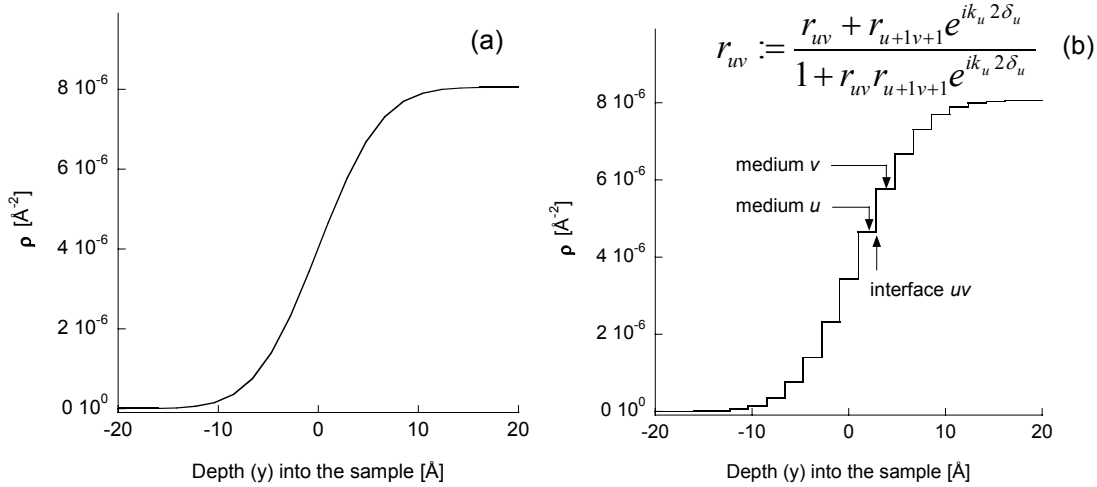**Figure 8 (a) Variation of the scattering length density profile of the air/Fe interface for σ = 5 Å is shown. (b) Approximation of the continuous function in (a) using discrete steps.**

There are two common approaches to calculate the (dynamical) reflectivity using the approximate scattering length density profile shown in Figure 8(a). The first approach, which is suitable for calculating the scattering length density profiles from scalar potentials (Equation 3 is an example of a scalar potential) is to use Equation 14 to calculate the reflection amplitude of the interface between the bottom-most thin slab and the infinitely thick substrate. Let the reflection amplitude of this interface be r_{mn} (bounded by Medium $m = n\text{-}1$ and Medium n—the substrate). Then, the reflection amplitude of the next higher interface— the $m\text{-}1m$-th interface, is computed using r_{mn} as the reflection amplitude of the phase-shifted term in Equation 14. This equation is applied recursively (as indicated in Figure 8(b) for the uv-th interface) until the top interface (the air/sample interface) is reached. Calculation of the reflectivity by recursively applying Equation 14 (for a particular $Q_\perp$) is required in order to properly account for dynamical scattering of the neutron beam by the sample surface at glancing angles. In other words, were the Born approximation a good representation of the scattering, then a recursive calculation to obtain the reflectivity curve would not be necessary. The recursive calculation is often referred to as the Parratt formalism [4].

The second approach to calculate the reflectivity curve is to generalize the matrix relation (Equation 12) for an arbitrary number of thin slabs, and then to solve the simultaneous equations to obtain the reflection amplitude of the ensemble (i.e., the entire sample). The second approach is one that can be used to calculate the reflection amplitude of a sample that might be represented by a scalar or vector potential (an example of a vector potential is one that includes the vector magnetization of a sample).

The matrix relation is generalized to the case of an any number of thin slabs as follows (for a detailed derivation see Ref. [28]):

$$\prod_{j=n-1}^{0} \overline{\overline{M_j(\delta_j)}} \begin{pmatrix} 1+r \\ ik_0(1-r) \end{pmatrix} = \begin{pmatrix} t \\ ik_n t \end{pmatrix} \prod_{j=n-1}^{0} e^{ik_n \delta_j} = \begin{pmatrix} t \\ ik_n t \end{pmatrix} e^{ik_n \Delta}$$

$$\overline{\overline{M_j(\delta_j)}} = \begin{pmatrix} \cos(k_j \delta_j) & \dfrac{1}{k_j}\sin(k_j \delta_j) \\ -k_j \sin(k_j \delta_j) & \cos(k_j \delta_j) \end{pmatrix}$$

$$\Delta = \sum_{j=1}^{n-1} \delta_j$$

<div align="right">**Equation 18**</div>

The subscript "j" in Equation 18 represents the j-th medium or slab. So, for example, k_j is the magnitude of the $\perp$-component of the wavevector in the j-th medium (see Equation 14), and δ_j is the thickness of the medium over which the scattering length density is considered constant [2 Å for the case of Figure 8(b)].

The reflectivity calculated for a 20 nm thick Fe film with roughened interfaces [whose scattering length density profile is shown in Figure 8(b)] is the solid curve in Figure 9. The case for the ideal Fe film [whose scattering length density profile is shown in Figure 5(b)] is the dashed curve in the figure.
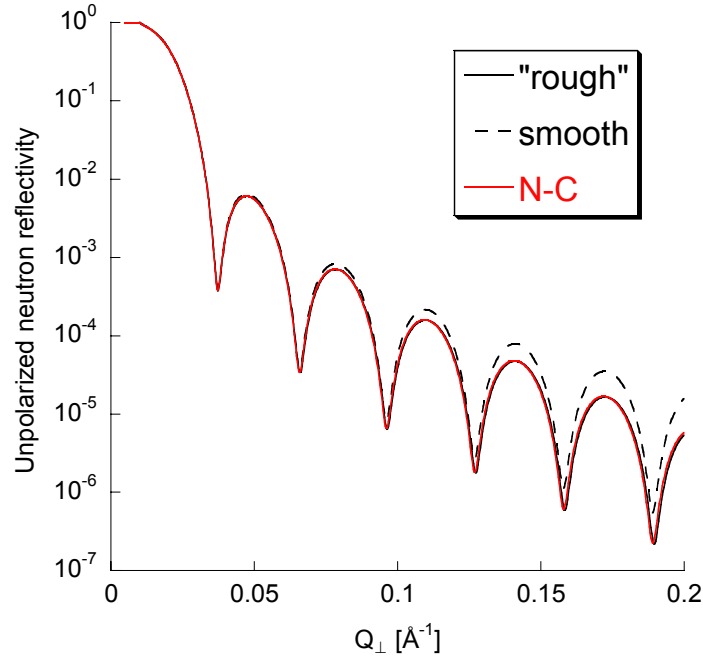
Figure 9 The influence of rough or diffuse interfaces is to attenuate the reflectivity with $Q_\perp$. The "rough" and "N-C" (computed using the Nevot and Croce relation) curves are essentially identical.

The reflectivity curve of a sample with rough or diffuse interfaces is attenuated more so than that of a smooth sample. The attenuation increases with $Q_\perp$. In fact, for the case of a single interface, Nevot and Croce [36] have analytically shown that the reflection amplitude of a single rough interface, r_r, having short length-scale roughness ($Q_\perp\sigma \ll 1$) is related to that of the ideal interface, r_i, by the relation:

$$r_r = r_i \exp\left(Q_\perp Q_\perp^t \sigma^2 / 2\right)$$

<div align="right">

Equation 19

</div>

where $Q_\perp^t$ ($= \mathbf{k}_{1f} - \mathbf{k}_{1i}$) is the wavevector transfer in the sample. As the kinematical limit is approached (i.e., $Q_\perp^t \rightarrow Q_\perp$), the attenuation factor is identical to a "static" Debye-Waller factor [37] (application of Equation 19 to the "smooth" curve in Figure 9 yields the red "N-C" curve). The important consequence of this observation is that interface roughness (or diffusion) will further limit the accessible region of wavevector transfer,

and consequently the sensitivity of reflectometry to changes of the scattering length density profile over thin layers. The attenuation of the reflectivity with roughness is a strong function of σ and $Q_\perp$; thus, more information can be extracted from samples with smooth interfaces than those with rough interfaces (although the physics of rough interfaces are often interesting!). For many experiments, useful information can be obtained from samples with (rms) interface roughness on the order of 10 Å, whereas, for samples with interface roughness of 20+ Å, success of the experiment may be hopelessly compromised.

The previous three theoretical examples have illustrated useful concepts and interpretations of reflectivity curves. The measurements and their interpretations are summarized in Table 2.

Table 2 Listing of measurements and the information yielded by the measurements.

Measurement feature	Information obtained from a sample of cm^2 or so size
Position of critical edge, Q_c	Nuclear (chemical) composition of the neutron-optically thick part of the sample, often the substrate.
Intensity for $Q < Q_c$	Unit reflectivity provides a means of normalization to an absolute scale.
Periodicity of the fringes	Provides measurement of layer thickness. Thickness measurement with uncertainty of 3% is routinely achieved. Thickness measurement to less than 1 nm can be achieved.
Amplitude of the fringes	Nuclear (chemical) contrast across an interface.
Attenuation of the reflectivity	Roughness of an interface(s) or diffusion across an

	interface(s). Attenuation of the reflectivity provide usually establishes a lower limit (typically of order 1-2 nm) of the sensitivity of reflectometry to detect thin layers.

Reflectometry with polarized neutron beams

In the previous section, neutron reflectometry was discussed in terms of the reflection of neutron beams from scattering potentials that are purely nuclear in origin. Since the neutron possesses an intrinsic magnetic moment and spin, the scattering potential may be spin dependent. There are two reasons that the interaction between a neutron and matter may depend on the neutron's spin. In some scattering processes (e.g., incoherent scattering of neutrons by hydrogen), the nuclear spin of an atom can interact with the spin of a neutron. On other occasions, the nuclei in a material from which the neutron scatters, may possess net spin and be polarized. Examples include spin polarized ^{3}He nuclei [38], or spin polarized Ga or As nuclei in the presence of a magnetic material [39]. The spin dependence of the potential for these examples involves two neutron scattering lengths, b^+ and b^-, where the sign of the term indicates whether the spin of the nuclei is parallel or anti-parallel to the laboratory magnetic field of reference (see Figure 1), which will later be identified with the polarization axis of the neutron beam.
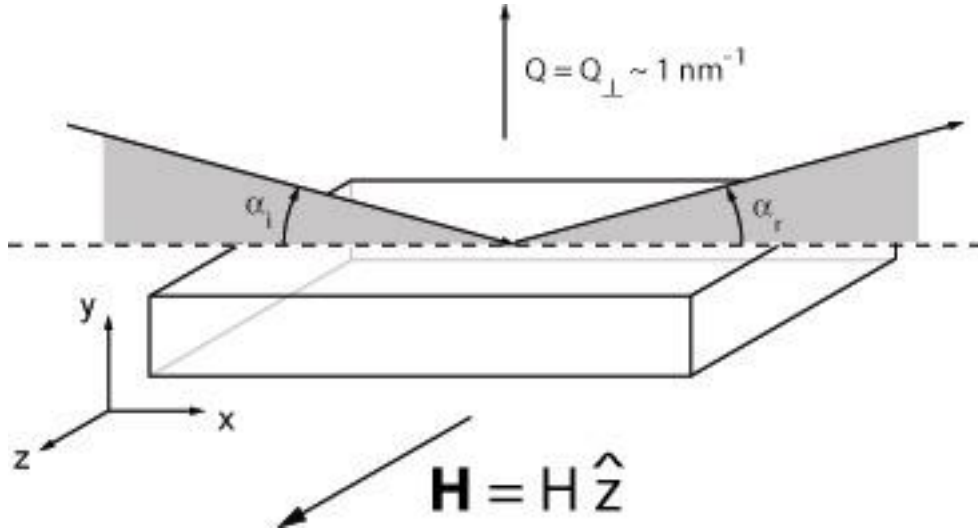
Figure 10 Diagram of a reflection experiment in which the sample is immersed in a magnetic field.

A commonly encountered second case involves the interaction of the neutron spin with atomic magnetism or other source of magnetic induction. The modification to the scattering potential (including the nuclear potential) is given by:

$$V = V_n + V_m = V_n \mp \underline{\mu} \cdot \boldsymbol{B}$$

<div align="right">

Equation 20
</div>

Here, $\boldsymbol{B}$ is the (spatially dependent) magnetic induction vector, and $\underline{\mu}$ is the magnetic moment of the neutron, where $\underline{\mu} = \mu_n \underline{\sigma}$, μ_n = -1.913 μ_N (the negative sign indicates that the neutron moment and its spin are anti-parallel), and $\underline{\sigma}$ is a linear combination of the (2 x 2) Pauli matrices [29] directed along each of the three orthogonal spatial axes with the magnetic field direction taken to lie along the $\hat{z}$-axis (Figure 10). The "$\mp$"-sign in Equation 20 is taken to be negative (positive) if the neutron spin is parallel (anti-parallel) to the laboratory field of reference ($\boldsymbol{H}$ in Figure 10). Since μ_n is negative, the quantity $-\mu_n B$ is positive, thus, adding to a normally positive nuclear scattering length—one for a repulsive potential (Mn, however, is an example of an atom

with a negative scattering length—an attractive potential). Fundamentally, the neutron spin interacts with magnetic induction, $\boldsymbol{B}$, so a materials-property that gives rise to $\boldsymbol{B}$, e.g., orbital and/or spin moments of atoms, or accumulation of spin in electronic devices, in principle can affect the neutron scattering process. The fact that the neutron spin interacts with magnetic induction and not magnetic field [40, 41, 42, 43] is fortunate, since were this not the case neutron scattering might not be a useful a tool in the study of magnetism.

Expressing the scattering potential V in matrix notation, we obtain [28]:

$$\overline{\overline{V(y)}} = \frac{2\pi\hbar^2}{m_n}\begin{pmatrix} \rho_n & 0 \\ 0 & \rho_n \end{pmatrix} \mp \mu_n \begin{pmatrix} B_z & B_x - iB_y \\ B_x + iB_y & -B_z \end{pmatrix}$$

Equation 21

The elements of the matrices are understood to depend on position, i.e., the nuclear scattering length density term, $\rho_n = \rho_n(y)$, etc. (in principle, dependence on x and z is also possible to observe with off-specular reflectometry). It is important to recognize that while most often the nuclear scattering potential outside of the sample is zero, $\rho_n = 0$, this is not necessarily the case for the magnetic induction. For example, in a polarized neutron reflectometry experiment, some magnetic field (as little as a couple Oe may be needed) is nearly always applied to the sample, in order to maintain the polarization of the neutron beam. Since neutron reflection occurs across interfaces with different scattering length densities (nuclear or magnetic), the *field* applied to the sample and the *field* inside the sample being the same do not yield contrast across the interface. Setting $\boldsymbol{B} = \mu_0\boldsymbol{H} + \boldsymbol{M}$, where $\boldsymbol{M}$ is the intensity of magnetization, and for fields applied along $\hat{z}$, Equation 21 can be rewritten as:

$$\overline{\overline{\delta V(z)}} = \frac{2\pi\hbar^2}{m_n}\begin{pmatrix} \rho_n & 0 \\ 0 & \rho_n \end{pmatrix} \mp \mu_n \begin{pmatrix} M_z & M_x - iM_y \\ M_x + iM_y & -M_z \end{pmatrix}$$

Equation 22 is a relation for the potential difference, $\overline{\overline{\delta V(z)}}$, between the sample and the surrounding medium (here, assumed to be air, but for cases in which the sample is not surrounded by air, the nuclear scattering length density of the surrounding medium must also be removed from ρ_n). The neutron magnetic scattering length density can be defined in terms similar to those used to define the neutron nuclear scattering length density (Equation 4).

$$\boldsymbol{\rho}_m = \sum_i^J N_i \boldsymbol{p}_i = C \sum_i^J N_i \boldsymbol{\mu}_i = C'\boldsymbol{m} = -\frac{m_n}{2\pi\hbar^2} \mu_n \sum_i^J \boldsymbol{M}_i$$

The units of the magnetic scattering length, $\boldsymbol{p}$, are Å. For the magnetic moment per formula unit, $\boldsymbol{\mu}$, expressed in units of μ_B, C = 2.645 x10^{-5} Åμ_B^{-1}. If, rather, the volume magnetization density, $\boldsymbol{m}$, is known in units of Tesla, then $C' = 2.9109$ x$10^{-5}/4\pi$ Å^{-2}T^{-1}; otherwise, for $\boldsymbol{m}$ in units of emu/cm^3, $C' = 2.853$ x10^{-9} Å^{-2}cm^3/emu. Substituting Equation 23 into Equation 22 yields:

$$\overline{\overline{\delta V(z)}} = \frac{2\pi\hbar^2}{m_n}\begin{pmatrix} \rho_n + \rho_{mz} & \rho_{mx} - i\rho_{my} \\ \rho_{mx} + i\rho_{my} & \rho_n - \rho_{mz} \end{pmatrix}$$

Finally, we associate the so-called non-spin-flip, ρ_{++} and ρ_{--}, and spin-flip scattering potentials, ρ_{+-} and ρ_{-+}, with the matrix elements in Equation 24.

$$\rho_{++} = \rho_n + \rho_{mz}$$

$$\rho_{--} = \rho_n - \rho_{mz}$$

$$\rho_{+-} = \rho_{mx} - i\rho_{my}$$

$$\rho_{-+} = \rho_{mx} + i\rho_{my}$$

$$\overline{\overline{\delta V(z)}} = \frac{2\pi\hbar^2}{m_n}\begin{pmatrix} \rho_{++} & \rho_{+-} \\ \rho_{-+} & \rho_{--} \end{pmatrix}$$

Equation 25

The "+" ("-") sign is for the neutron spin parallel (anti-parallel) to the applied field, so the positive magnetic scattering potential adds to the normally positive (repulsive) nuclear scattering potential. So, for example, ρ_{++} is the element of the scattering potential attributed to the scattering of an incident neutron with spin-up that does not change the orientation of the neutron spin with respect to the magnetic field. Likewise, ρ_{+-} is the element of the scattering potential attributed to the scattering of an incident neutron that changes its spin from up to down, and so on.

We now desire a solution to Schrödinger's equation—one that takes into account the spin dependence of the scattering potential (Equation 25) and the spin dependence of the neutron wave function:

$$\Psi(y) = U_+\begin{pmatrix} 1 \\ 0 \end{pmatrix}\Psi_+(y) + U_-\begin{pmatrix} 0 \\ 1 \end{pmatrix}\Psi_-(y)$$

$$\Psi_+(y) = e^{ik_+ y}$$

$$\Psi_-(y) = e^{ik_- y}$$

Equation 26

The value of $k_\pm$ is for the $\perp$-component (or y-component in Figure 10) of the wavevector for the different neutron spin states. The spin dependence of $k_\pm$ arises from the energy dependence of the neutron spin in the magnetic field. In the field, the refractive index becomes spin-dependent (i.e., birefringent).

$$k_{\pm} = n_{\pm}k_0 = \sqrt{1 - \frac{4\pi\left(\rho_n \pm |\boldsymbol{\rho}_m|\right)}{k_0^2}}k_0$$

The spin dependence of the incident neutron wave function contained in U_+ and U_- is determined by the polarization of the incident neutron beam.

Theoretical Example 4: Reflection of a polarized neutron beam from a magnetic film

In this example, we consider the reflection of a polarized neutron beam from a magnetic thin film in which the direction of magnetic induction is uniform. This example illustrates how the Parratt formalism developed earlier for unpolarized neutron reflection can be straightforwardly applied to a (saturated) magnetic thin film. Since the direction of magnetic induction is assumed to be parallel to the applied field, and the direction is uniform throughout the film (though the magnitude of the induction need not be uniform), the off-diagonal entries in the matrix of Equation 25 are zero. We now imagine performing an experiment involving two measurements of the sample reflectivity; first with spin-up neutrons (so $U_+ = 1$ and $U_- = 0$), and then later with spin-down neutrons (so $U_+ = 0$ and $U_- = 1$). A device called a spin-flipper (discussed later) flips the neutron spins from one state to the other. Equation 18 is easily generalized to account for the spin dependence of the neutron scattering potential [28].

$$\prod_{j=n-1}^{0} \overline{\overline{M_j^{\pm}(\delta_j)}} \begin{pmatrix} 1 + r_{\pm} \\ ik_0(1 - r_{\pm}) \end{pmatrix} = \begin{pmatrix} t_{\pm} \\ ik_{\pm n}t_{\pm} \end{pmatrix} \prod_{j=n-1}^{0} e^{ik_{n\pm}\delta_j} = \begin{pmatrix} t_{\pm} \\ ik_{\pm n}t_{\pm} \end{pmatrix} e^{ik_{\pm n}\Delta}$$

$$\overline{\overline{M_j^{\pm}(\delta_j)}} = \begin{pmatrix} \cos(k_{\pm j}\delta_j) & \frac{1}{k_{\pm j}}\sin(k_{\pm j}\delta_j) \\ -k_{\pm j}\sin(k_{\pm j}\delta_j) & \cos(k_{\pm j}\delta_j) \end{pmatrix}$$

In the previous example of a thin Fe layer on Si, we had considered the 20 nm thick layer to be a non-magnetic material with the nuclear scattering length density of Fe. Now, we consider the Fe to be fully saturated with magnetization parallel to the field as shown in Figure 10. The magnetic moment of an Fe atom is μ_{Fe} = 2.219 μ_B, so the neutron magnetic scattering length density is $\rho_m = N_{Fe}C\mu_{Fe} = 4.97x10^{-6}$ Å^{-2} (Table 1). The scattering length density profiles for spin-up and spin-down neutrons are shown in Figure 11(a), as is the profile of the nuclear scattering length density [Figure 7(a)] alone for the sake of comparison. Depending upon whether the polarization of the neutron beam is parallel or anti-parallel to $\boldsymbol{H}$, ρ_m either adds or subtracts from ρ_n. The reflectivities for spin-up neutrons, R^{++} [for which the blue curve in Figure 11(a) is appropriate], and spin-down neutrons, R^{--}, [for which the red curve in Figure 11(a) is appropriate] are shown in Figure 11(b). The dotted curve in Figure 11(b) is the reflectivity of a non-magnetic film with the nuclear scattering length density of Fe (Figure 7), and would not be measured from a magnetized film of Fe with polarized neutron beams. In this example, the splitting between the R^{++} and R^{--} is a measure of the depth profile of the sample magnetization projected onto the applied field direction.
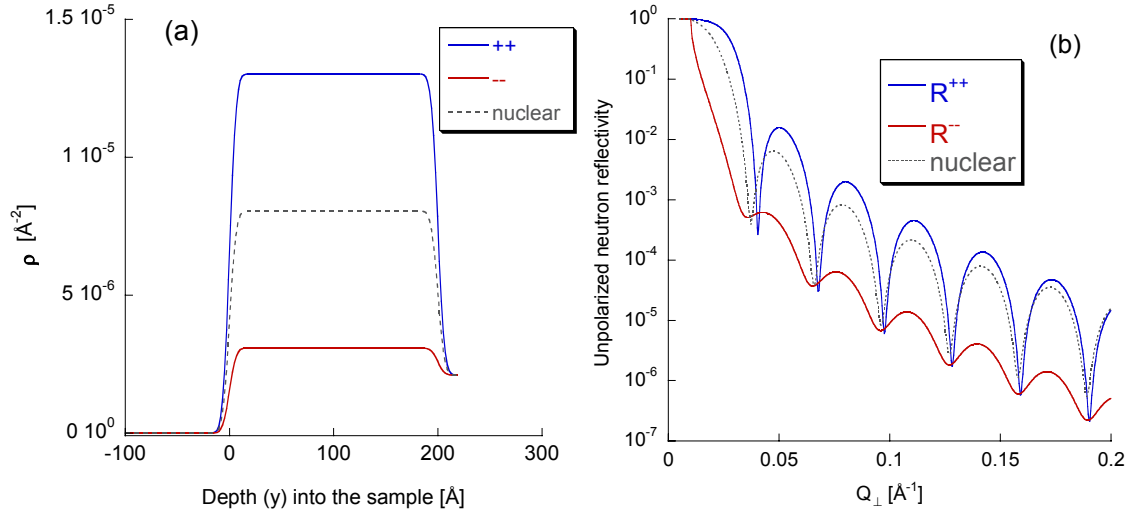
Figure 11 (a) Bifurcation of the magnetic scattering length densities profiles depending upon whether the neutron spin is parallel (++, blue curve) or anti-parallel (--, red curve) to the direction of the applied magnetic field. The dotted curve is the nuclear scattering length density profile. (b) The R^{++} and R^{--} reflectivity of the sample is shown as the blue and red curves, respectively. The dashed curve is the reflectivity curve for the case of a film with the nuclear scattering length density of Fe (and not magnetic).

Influence of imperfect polarization on reflectivity curves

In the preceding discussions, reflectivity curves were calculated for neutron beams that were assumed to contain only spin-up neutrons or spin-down neutrons. In other words the neutron beams were ideally polarized. In practice, the polarization of a neutron beam,

$$P = \frac{I_+ - I_-}{I_+ + I_-}$$

Equation 29

where I_+ and I_- represent the numbers or fractions of spin-up and spin-down neutrons, respectively, is not 100%. Typically, polarizations of order 90+ % are available for reflectometry experiments.

In order to produce a polarized neutron beam, polarization devices (discussed later) are inserted into the beam line before and sometimes after the sample. A

polarization device acts to suppress one spin state by either absorbing the undesired spin state (such a device is often called a polarization filter), or by spatially separating the two spin states through reflection from magnetized materials. Nearly all polarized neutron beams contain some fraction of undesired spins. Assume the desired spin state is the spin-up state. The contamination of the polarized neutron beam is attributed to spin-down neutrons. The polarization of the neutron beam approaches 100%, when the ratio, called the flipping ratio $F = \dfrac{I_+}{I_-}$, of desired neutron spins to undesired neutrons spins becomes large, in fact:

$$P = \frac{F-1}{F+1}$$

Equation 30

Since the transmission of a neutron beam through polarizing supermirrors is typically reduced by about 30% due to absorption of the beam by the Si substrates and Co in the coatings, experimentalists are best served by neutron beams with just enough polarization to obtain the data needed to solve a problem. Somewhat counter-intuitively, it may sometimes be more advantageous to study highly magnetic materials with higher neutron polarizations than used for materials that are only slightly magnetic. To understand this point, we assume that rather than using the perfectly polarized neutron beam in Theoretical Example 4, we use one having a flipping ratio of 10 (i.e., 1 in 10 neutrons has the wrong spin state, $P = 82\%$). The as-measured spin-up reflectivity will be composed of $0.9R^{++}$ [Figure 11(b)] and $0.1R^{--}$ [Figure 11(b)], which hardly changes the result (compare the solid and dashed blue curves in Figure 12). However, since the spin-up reflectivity is so much larger than the spin-down reflectivity (in this example),

the as-measured spin-down reflectivity will consist of $0.1R^{++}$ (a large source of contamination) and $0.9R^{--}$ (compare the solid and dashed red curves in Figure 12). Failure to account for imperfection of the polarized neutron beam would lead one to mistakenly conclude that the Fe film was less magnetic than it actually is. Provided the polarization of the neutron instrument is known, the true reflectivity curves can be obtained from reflectivity measurements using neutron beams with less than 100% polarization [44].
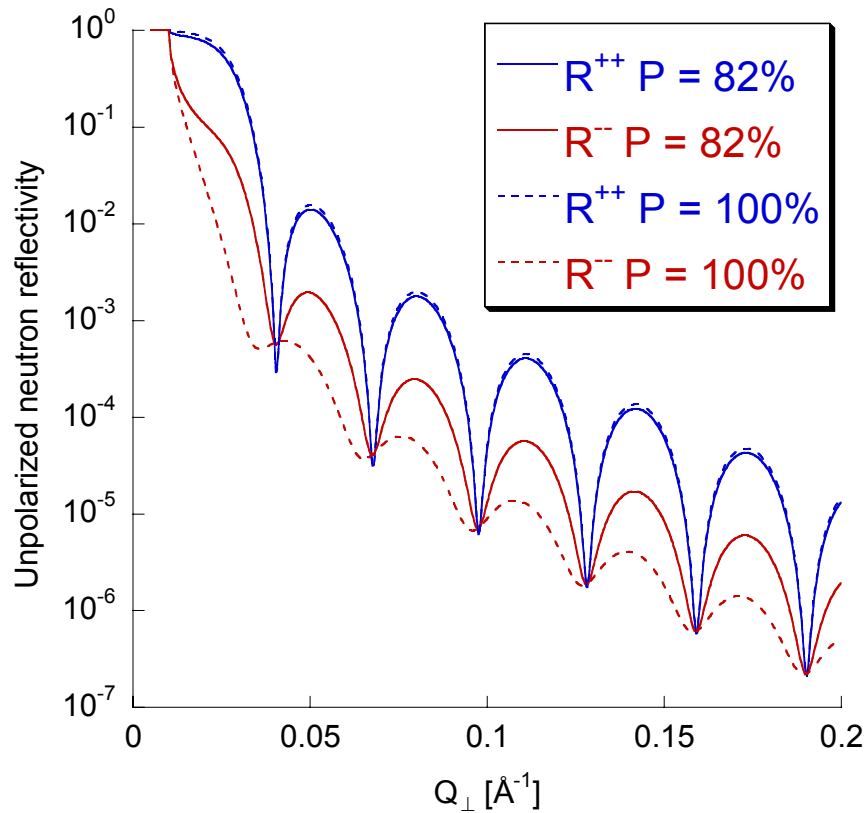

Figure 12 Reflectivity curves calculated for an ideally polarized neutron beam (dashed curves) are compared to those calculated for a neutron beam with 82% polarization (solid curves). The large spin-up reflectivity (blue curve) is hardly affected by a poorly polarized neutron beam. On the other hand, the contamination in the poorly polarized neutron beam greatly perturbs the much weaker spin-down reflectivity (red curve), because the contamination when measuring spin-down is spin-up and the spin-up reflectivity is much larger than the spin-down reflectivity.

In contrast, for the case of a material that is only weakly magnetic, e.g., a magnetic semiconductor with magnetization ~ 30 emu/cm^3, R^{++} and R^{--} will be little

different, so the contamination posed by having $1/10^{th}$ of the wrong spin state in the as-measured reflectivity might be negligible. In this situation, a relatively poorly polarized neutron beam might be preferred over a highly polarized neutron beam, especially if the intensity of the poorly polarized neutron beam is larger than that of the highly polarized beam.

"Vector" magnetometry with polarized neutron beams

In the previous discussions, the neutron spin and magnetic induction have been treated as if they were always parallel (or anti-parallel) to the neutron spin direction. However, this constraint does not always exist. For example, a material with strong uniaxial anisotropy could be oriented with M at an angle of ϕ to H (Figure 13). Classically, when a neutron whose spin enters a region in which its spin is not parallel to the induction, the neutron spin begins to precess. Depending upon the time the neutron spends in this region and the strength of the induction, the neutron spin may flip 180°—the intentional rotation of a neutron spin by 180° is the basis for operation of a so called Mezei spin-flipper [45]. Likewise, the magnetization of a material can rotate the spin of a neutron such that a beam with one polarization scatters from the sample with diminished polarization, i.e., some of the spin-up neutrons may be flipped to spin-down—so-called spin-flip scattering. In this situation, the scattering potential, $\overline{\overline{\delta V(z)}}$, is not simply birefringent: in other words the off-diagonal elements in Equation 25 are non-zero.
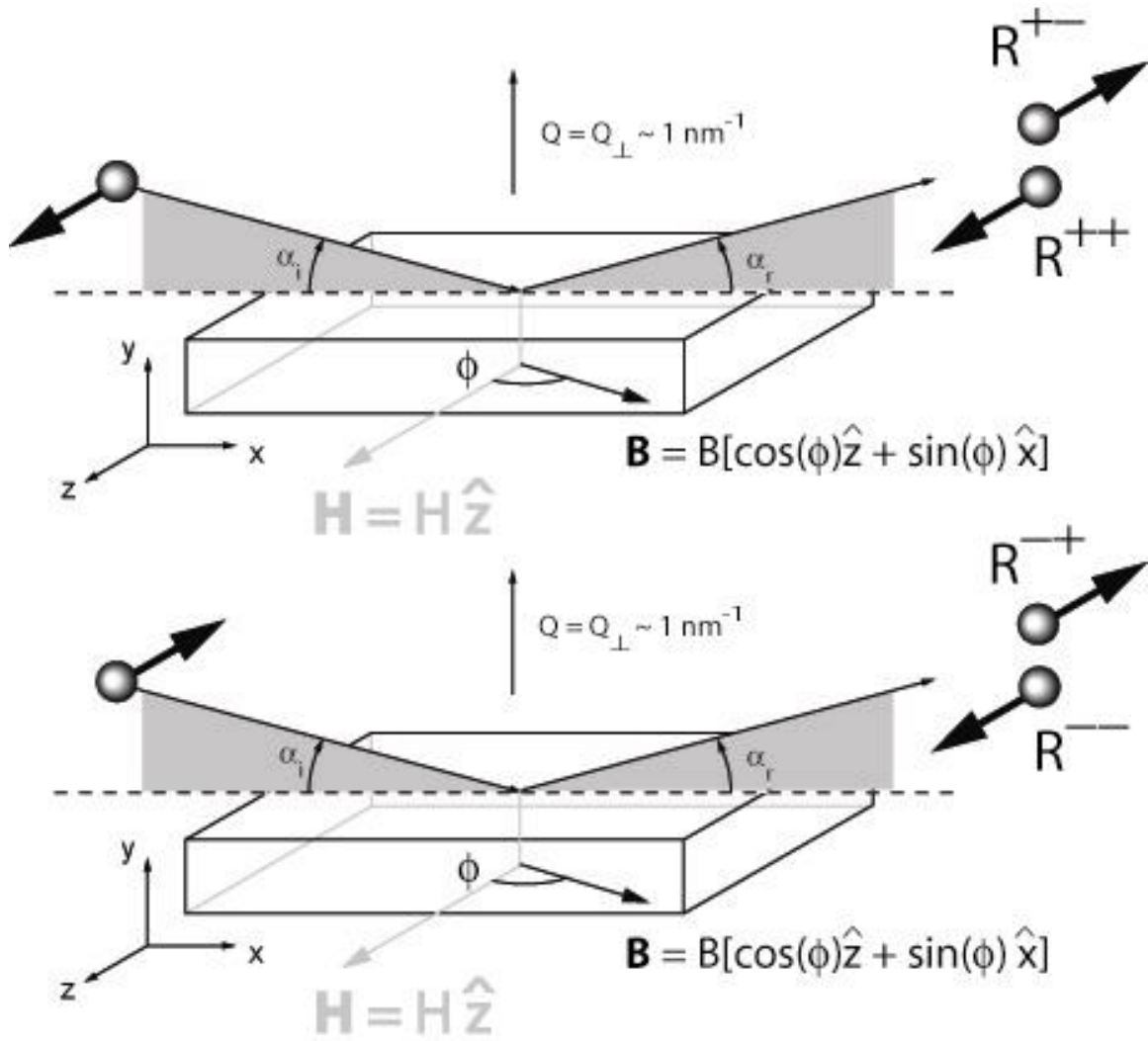
Figure 13 Schematic diagram showing (top) a spin-up polarized neutron beam reflecting from a sample with magnetic induction at an angle of ϕ from the applied field. The reflected beam has two components—the (R^{++}) non-spin-flip and (R^{+-}) reflectivities. (lower) The case is shown when the polarization of the incident neutron beam is spin-down.

For the geometry of the neutron reflectometry experiment shown in Figure 13, a further simplification to the off-diagonal elements of Equation 22 can be made. One of Maxwell's equations (specifically $\nabla \cdot \boldsymbol{B} = 0$ [46]) requires the out-of-plane component of $\boldsymbol{B}$ across the interface to be continuous, so the component of $\boldsymbol{B}$ parallel to $\boldsymbol{Q}$ or $\hat{y}$ will not yield a change in contrast across the interface; therefore, $\rho_{+-} = \rho_{-+} = \rho_{mx} \equiv \rho_{SF}$. The

important consequence of the dipolar interaction between neutron and magnetic moments is that magnetic scattering of the neutron is only produced by the component of the magnetization perpendicular to wavevector transfer. In the case of a (specular) neutron reflection experiment (Figure 13), this requirement means that spin-dependence of the neutron reflectivity arises from the components of the sample magnetization projected onto the reflection (or sample) plane.

Theoretical Example 5: Reflection from a magnetic medium in which the direction of magnetic induction is perpendicular to the applied field and parallel to the plane of the sample

We now calculate the scattering from the Fe film for the case when the Fe magnetization is rotated through an angle ϕ about the surface normal from the applied field direction (see Figure 13). In order to account for the possibility that the sample changes the spin state of a neutron, a generalization of Equation 28 to include spin-flip scattering, is required [19, 20, 28].

$$\prod_{j=n-1}^{0} \overline{\overline{A_j}} \begin{pmatrix} I_+ + r_+ \\ I_- + r_- \\ ik_0(I_+ - r_+) \\ ik_0(I_- - r_-) \end{pmatrix} = \begin{pmatrix} t_+ \\ t_- \\ ik_n t_+ \\ ik_n t_- \end{pmatrix}$$

Equation 31

where the elements of $\overline{\overline{A_j}}$ are:

$$A_{11} = 2\eta\left[\gamma_3 \cosh(S_+\delta_j) - \gamma_1 \cosh(S_-\delta_j)\right]$$

$$A_{21} = 2\eta\left[\gamma_1\gamma_3 \cosh(S_+\delta_j) - \gamma_1\gamma_3 \cosh(S_-\delta_j)\right]$$

$$A_{31} = 2\eta\left[S_+\gamma_3 \cosh(S_+\delta_j) - S_-\gamma_1 \cosh(S_-\delta_j)\right]$$

$$A_{41} = 2\eta\left[S_+\gamma_1\gamma_3 \cosh(S_+\delta_j) - S_-\gamma_1\gamma_3 \cosh(S_-\delta_j)\right]$$

$$A_{12} = 2\eta\left[-\cosh(S_+\delta_j) + \cosh(S_-\delta_j)\right]$$

$$A_{22} = 2\eta\left[-\gamma_1 \cosh(S_+\delta_j) + \gamma_3 \cosh(S_-\delta_j)\right]$$

$$A_{32} = 2\eta\left[-S_+ \sinh(S_+\delta_j) + S_- \sinh(S_-\delta_j)\right]$$

$$A_{42} = 2\eta\left[-S_+\gamma_1 \sinh(S_+\delta_j) + S_-\gamma_3 \sinh(S_-\delta_j)\right]$$

$$A_{13} = 2\eta\left[\frac{\gamma_3}{S_+}\sinh(S_+\delta_j) - \frac{\gamma_1}{S_-}\sinh(S_-\delta_j)\right]$$

$$A_{23} = 2\eta\left[\frac{\gamma_1\gamma_3}{S_+}\sinh(S_+\delta_j) - \frac{\gamma_1\gamma_3}{S_-}\sinh(S_-\delta_j)\right]$$

$$A_{33} = A_{11}$$

$$A_{43} = A_{21}$$

$$A_{14} = 2\eta\left[-\frac{1}{S_+}\sinh(S_+\delta_j) + \frac{1}{S_-}\sinh(S_-\delta_j)\right]$$

$$A_{24} = 2\eta\left[-\frac{\gamma_1}{S_+}\sinh(S_+\delta_j) + \frac{\gamma_3}{S_-}\sinh(S_-\delta_j)\right]$$

$$A_{34} = A_{12}$$

$$A_{44} = A_{22}$$

and

$$S_\pm = in_\pm k_0$$

$$\gamma_1 = \frac{|\boldsymbol{\rho}_m| - \rho_{mz} + \rho_{mx} + i\rho_{my}}{|\boldsymbol{\rho}_m| + \rho_{mz} + \rho_{mx} - i\rho_{my}}$$

$$\gamma_3 = \frac{|\boldsymbol{\rho}_m| + \rho_{mz} - \rho_{mx} - i\rho_{my}}{|\boldsymbol{\rho}_m| - \rho_{mz} - \rho_{mx} + i\rho_{my}}$$

$$2\eta = \frac{1}{\gamma_3 - \gamma_1}$$

Equation 32

To calculate the four neutron spin reflectivities, R^{++}, R^{+-}, R^{-+} and R^{--}, the nuclear

(ρ_n) and magnetic ($\boldsymbol{\rho}_m$, a vector) scattering length density profiles for the sample are

computed.   Examples of these profiles are shown in Figure 14, where

$$\boldsymbol{\rho}_m = C'm_{Fe}\left(\cos(\phi)\hat{z} + \sin(\phi)\hat{x}\right).$$

Next, we assume the sample is illuminated by a spin-up polarized neutron beam,

so $I_+ = 1$ and $I_- = 0$, and use Equation 31 to compute R^{++} and R^{+-} ($\equiv |r_+|^2$ and $|r_-|^2$; the

probabilities that a neutron with up-spin is reflected with up-spin or down-spin,

respectively).   Then, the calculation is repeated for a spin-down polarized neutron beam

($I_+ = 0$ and $I_- = 1$) to obtain R^{-+} and R^{--} ($\equiv |r_+|^2$ and $|r_-|^2$; the probabilities that a neutron

with down-spin is reflected with up-spin or down-spin, respectively). The result is plotted

in Figure 15, where $R^{SF} = \dfrac{R^{+-} + R^{-+}}{2}$, for the cases (a) $\phi = 90°$ and (b) $\phi = 45°$. For the

case $\phi = 90°$, the net magnetization of the sample along the applied field is zero, so there

is no splitting between the two non-spin-flip cross-sections (and a strong signal in the

spin-flip cross-section).   On the other hand, for $\phi = 45°$, the net magnetization of the

sample along the applied field is non-zero, so splitting between R^{++} and R^{--} is observed

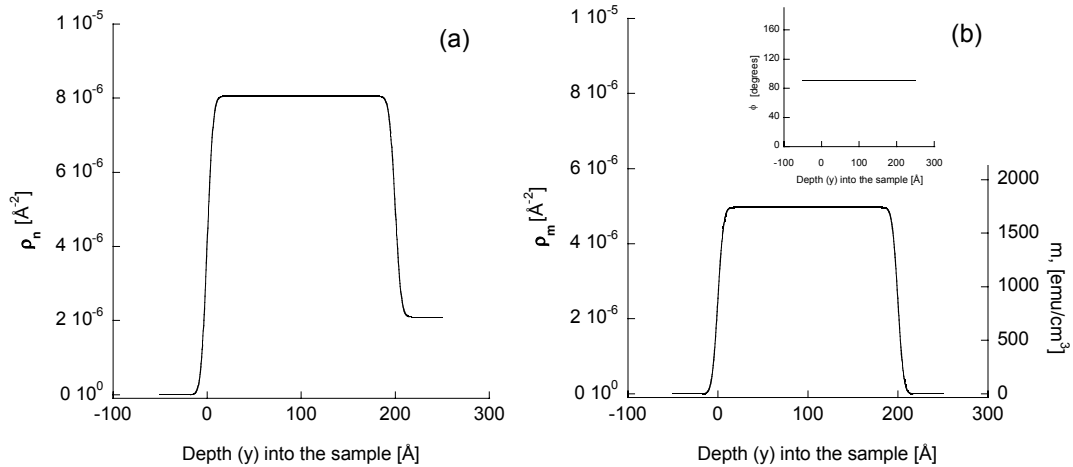along with a lower magnitude for R^{SF}.

Figure 14 Plot of the nuclear (a) and magnetic (b) scattering length densities profiles. Inset: The angle about the surface normal of the magnetization from the applied field is 90°.
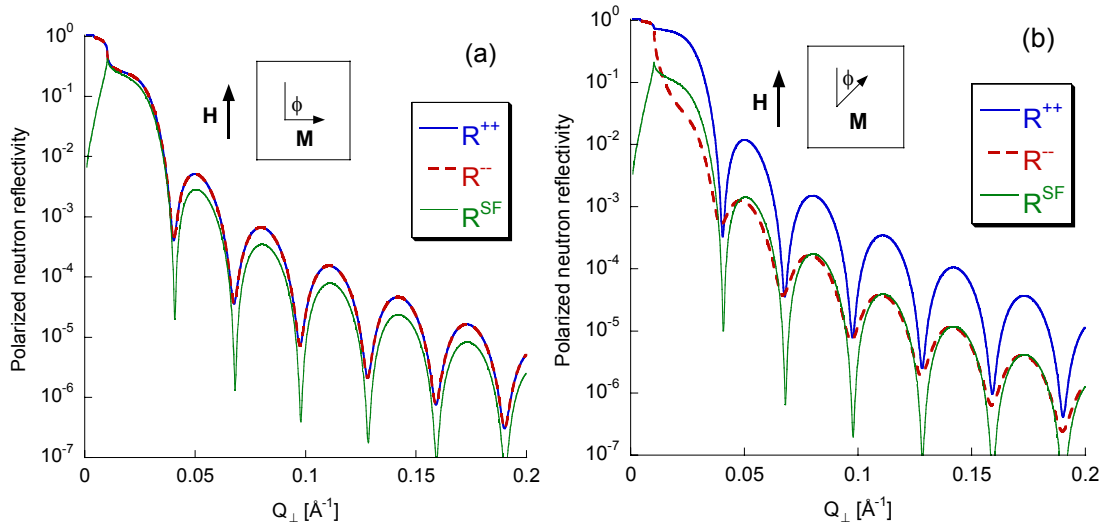

Figure 15 Polarized neutron reflectivity curves for the Fe/Si sample (inset) with Fe magnetization rotated (a) $\phi = 90°$ and (b) $\phi = 45°$ from the applied field and polarization axis of the neutron beam.

A qualitative (and intuitive) understanding of "vector" magnetometry

An intuitive understanding of spin-dependent reflection is most easily obtained by considering the kinematical equations that describe reflection, which so far has been treated using the exact dynamical formalism. By kinematical, we mean that effects such as the evanescence of the wave function below the critical edge, which greatly perturb the wave function inside the sample, are negligible. These effects are neglected when the

transmitted wave function in Equation 1 is replaced with the incident wave function. Within the Born approximation, the spin-dependent reflection amplitudes for the scattering geometry shown in Figure 13 are [28]:

$$r_{BA}^{\pm\pm}(Q_\perp) \propto \int_0^\Delta [\rho_n(y) \pm \rho_m(y)\cos\phi(y)]e^{iQ_\perp y}dy$$

$$r_{BA}^{\pm\mp}(Q_\perp) \propto \int_0^\Delta \rho_m(y)\sin\phi(y)e^{iQ_\perp y}dy$$

Equation 33

The reflectivities for the non-spin-flip processes are a sum of the squares of the nuclear and magnetic structure factors (given in Equation 33) plus a term resulting from the interference between nuclear and magnetic scattering. The interference term is observed with polarized neutron beams. The spin-flip reflectivity is purely magnetic in origin. Note for the special case where $\phi = 90°$, as can be realized for samples with uniaxial anisotropy, the non-spin-flip reflectivities are purely nuclear (or chemical) in origin. In this special case, the magnetic and chemical profiles of the sample can be isolated from one another. By measuring both the non-spin-flip and spin-flip reflectivities as a function of $Q_\perp$, Equation 33 suggests that the variation of the magnetization vector, in amplitude and direction in the sample plane, can be obtained as a function of depth. This capability is an important reason why polarized neutron reflectometry complements conventional vector magnetometry, which is a technique that measures the net (or average) magnetization vector of a sample.

A second important example of the power of polarized neutron reflectometry is for detecting and isolating magnetism of weakly magnetic materials from that of strongly magnetic materials through analysis of the Fourier components in the reflectivity curves.

Situations in which this capability may be valuable include detecting coerced or proximal magnetism in materials that are normally non-magnetic in the bulk, e.g., Pd that becomes magnetic in proximity to Fe [47]. Polarized neutron reflectometry is also valuable in studies of weakly ferromagnetic thin films, e.g., (Ga, Mn)As [48], grown on substrates that contribute a strong diamagnetic or paramagnetic background to the signal measured in a conventional magnetometer.

For studies of films whose magnetization does not change with depth, but instead the magnetization changes along the film plane, as realized for example in films composed of magnetic domains, the sizes of the magnetic domains in relation to the coherence of the neutron beam (which is typically microns in size) determine whether off-specular or diffuse scattering of the neutron beam, in addition to specular scattering, is observed. Diffuse scattering can be observed when the lateral variation of the magnetization is small in comparison to the coherence of the neutron beam. On the other hand, if the domains are much bigger than the coherence of the beam, then information about the magnetism of the sample will be observed in the specular reflectivity.

Consider reflection of a neutron beam from a single domain with uniform magnetization and having a lateral size that is large in comparison to the coherent region of the neutron beam. In this example, the reflectivity of the domain is straightforwardly calculated using Equation 33.

$$R_{BA}^{\pm\pm}(Q_\perp) \propto \left(\rho_n^2 + \rho_m^2 \cos^2\phi \pm 2\rho_n\rho_m \cos\phi\right)\left(1 - \cos Q_\perp \Delta\right)$$
$$R_{BA}^{SF}(Q_\perp) = R_{BA}^{\pm\mp} \propto \rho_m^2 \sin^2\phi\left(1 - \cos Q_\perp \Delta\right)$$

Equation 34

47

Using the relation between ρ_m and $\boldsymbol{m}$ provided by Equation 23 we resolve $\boldsymbol{m}$ into components parallel and perpendicular to the applied field such that $m_{\parallel} \propto \rho_m \cos \phi$ and $m_{\perp} \propto \rho_m \sin \phi$, respectively. Then, using Equation 34 we obtain a physical meaning for the difference (or splitting) between the non-spin-flip reflectivities, Δ_{NSF}, and R^{SF}.

$$\Delta_{NSF}(Q_{\perp}) = R_{BA}^{++}(Q_{\perp}) - R_{BA}^{--}(Q_{\perp}) \propto m_{\parallel}\left(1 - \cos Q_{\perp}\Delta\right)$$
$$R_{BA}^{SF}(Q_{\perp}) \propto m_{\perp}^2\left(1 - \cos Q_{\perp}\Delta\right)$$

<div align="right">**Equation 35**</div>

That is, the splitting between the non-spin-flip reflectivities is proportional to the projection of the domain magnetization onto the applied field, and the spin-flip reflectivity is proportional to the *square* of the domain magnetization perpendicular to the applied field.

Owing to the fact that neutron scattering is a statistical probe of a sample's potentially non-uniform distribution of magnetization, rather than a scanning probe of the magnetization at the atomic scale (which could be non-representative), there is an important complication to the interpretation of the neutron scattering results. The complication stems from, as discussed earlier, whether the non-uniformity of magnetization varies on a length scale that is small or large compared to the coherent region [49] of the neutron beam. If the fluctuations of magnetization are small compared to the coherent region of the neutron beam, then the reflectivity is obtained from the reflection amplitude of an ensemble of domains. Depending upon the details of the fluctuations, the scattering may consist of specular and off-specular (or diffuse scattering) components. On the other hand, if the fluctuations occur on a length scale larger than the

coherent region of the neutron beam, then the reflectivity is the sum of the reflectivity of each component and the reflectivity is specular.

It is the second case, one composed of domains that are large in comparison to the coherent region of the neutron beam that is easiest to treat. In this case, $\Delta_{NSF} \propto \langle m_\parallel \rangle$ and $R_{BA}^{SF} \propto \langle m_\perp^2 \rangle$, where $\langle \ \rangle$ denotes the average value of the ensemble. The first term, Δ_{NSF}, provides a measure of the Fourier components of the net sample magnetization projected onto the applied field and is similar to the net magnetization of the sample as measured by a magnetometer (in a sense a magnetometer measures Δ_{NSF} corresponding to $Q_\perp = 0$). The second term contains qualitatively different information than that which can be measured by a vector magnetometer. Specifically, R^{SF} is a measure of the *mean square deviation* of the magnetization away from the applied field. For the examples of magnetic domain distributions shown in Figure 16, the net sample magnetization in any direction is zero. In this situation, a vector magnetometer would measure the zero-vector, yet, provided the domains are large in comparison to the coherence of the neutron beam, the mean square deviation of the magnetization away from the applied field is a (non-zero) quantity obtained from polarized neutron scattering as R^{SF} [50]. Note, f_1, $f_\perp = f_2 + f_4$, and f_3 [Figure 16(left)] and ϕ [Figure 16(right)] can be chosen such that $\langle m_\perp^2 \rangle$ is the same for both models, so polarized neutron reflectometry cannot distinguish between these two particular domain distributions, nevertheless the technique does provide information about magnetic properties, e.g., anisotropy [51] that are related to $\langle m_\perp^2 \rangle$.

Extreme cases of domain distributions—ones that yield no net magnetization along the applied field (as realized when the magnitude of the applied field is equal to the

coercive field) are shown in Figure 17, along with the features of the *specular* reflectivity curves that are unique to the particular domain structure. In the first case, the non-spin-flip reflectivities would be superimposed with amplitudes that contain nuclear and magnetic contributions [the reflectivity curve would not be the same as the purely nuclear case shown in Figure 5(b)]. The period of the non-spin-flip reflectivities would be $2\pi/\Delta$, and the spin-flip reflectivity would be zero. In the second case, the non-spin-flip reflectivities would be purely nuclear in origin, and the spin-flip reflectivity would be non-zero with a period equal to the $2\pi/\Delta$. In the third case, the two non-spin-flip reflectivities would be different and have a period of $2\pi/(\Delta/2)$. The spin-flip reflectivity would be zero for this case. For the last case, the non-spin-flip reflectivities would be purely nuclear in origin (as in the second case) and the spin-flip reflectivity would be non-zero with a period of $2\pi/(\Delta/2)$.
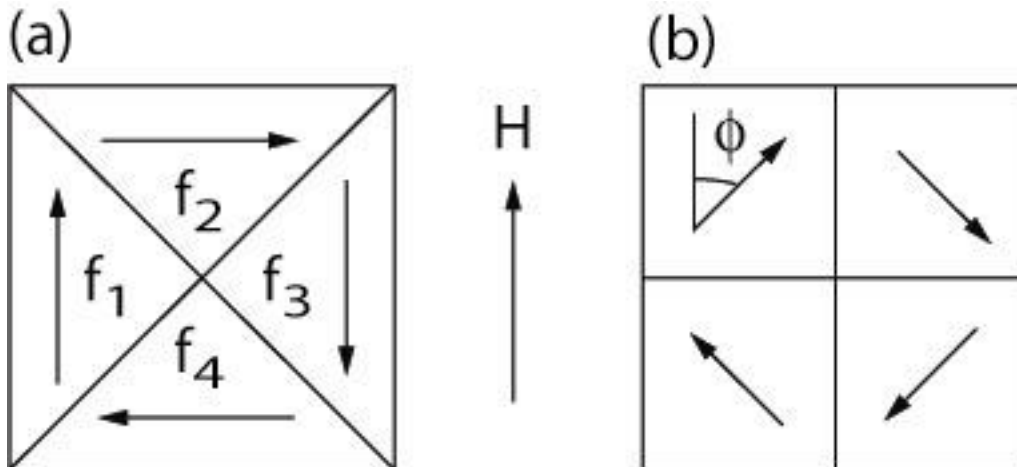

Figure 16 Examples of magnetic domains with magnetization directed as shown by the arrows. (a) In this closure domain model f_i represents the area fraction of the i-th domain, and the magnetization of the material reverses by changing the value of f_i. (b) In this model, the area fractions of the domains are equal and the magnetization of the material reverses as the angle between the magnetization and the applied field direction changes from 0 to 180°.
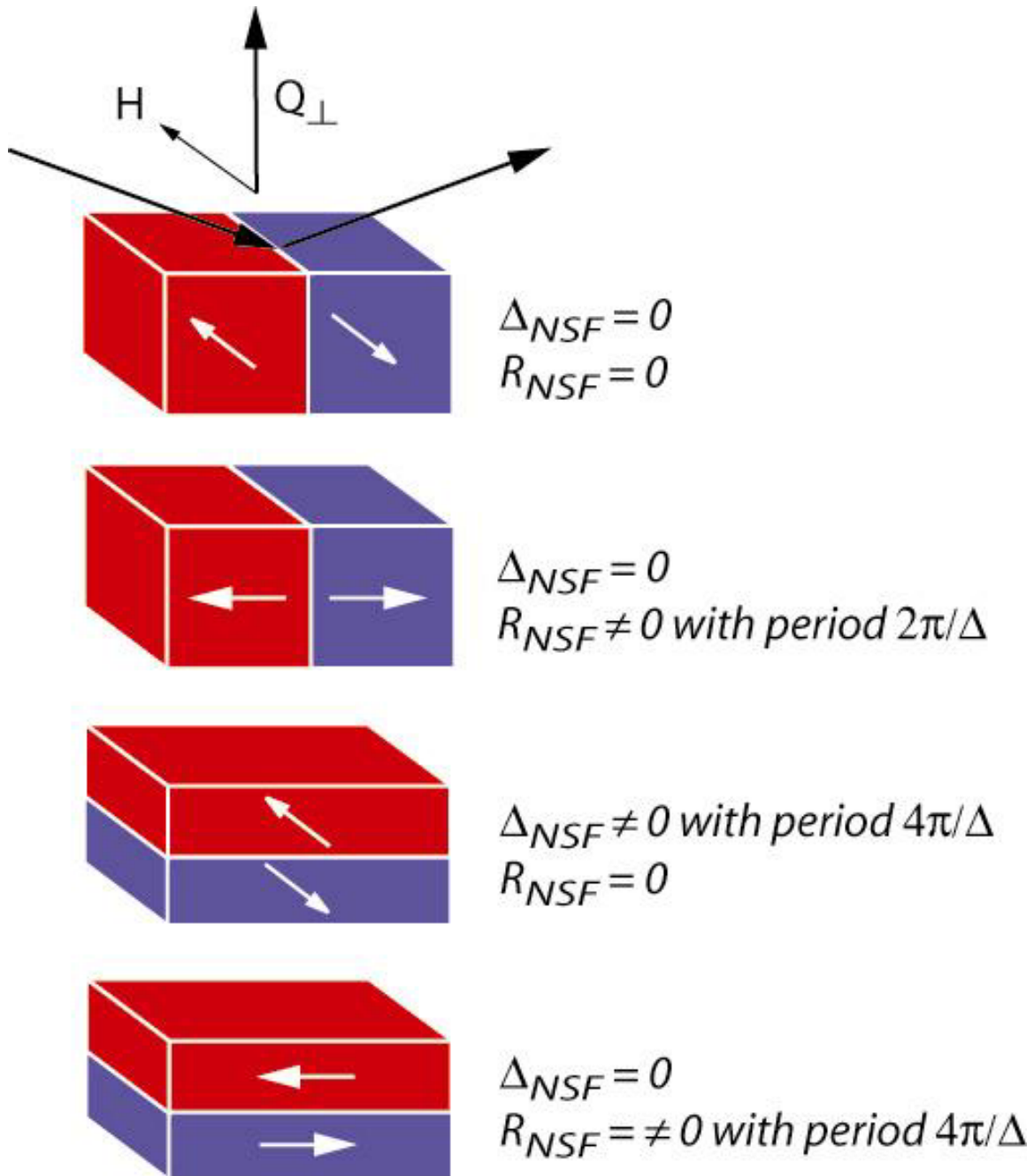
Figure 17 Four examples of a magnetic material whose net magnetizations along the applied field, H, (or any direction) are all zero (the volume fractions of red and blue domains are equal, and the domain sizes are assumed to be large in comparison to the coherent region of the neutron beam). The neutron scattering signature in the specular reflectivities from each model is unique.

Description of a polarized neutron reflectometer

Three essential requirements for any polarized neutron reflectometer are:

(1) an a priori knowledge of the polarization of the neutron beam illuminating the sample;

(2) the capability to measure the intensity and polarization of the neutron beam reflected by a sample;

(3) and the ability to make these measurements as a function of wavevector transfer parallel and perpendicular to the sample surface.

The first feature requires a device to polarize the neutron beam (a polarizer) and to flip the neutron beam polarization (a spin-flipper). The second feature requires a neutron detector and a device(s) to flip and measure the neutron beam polarization after reflection from the sample. Finally, wavevector transfer is obtained from measurements of the neutron wavelength and the angle through which the neutron has been scattered. Angles are measured using slits to define the path of the neutron beam that is allowed to strike a neutron detector, or by using a position sensitive neutron detector.